Automated quantification of synaptic boutons reveals their 3D distribution in the insect mushroom body

Amélie Cabirol[1], Albrecht Haase[1, 2]*

[1]Center for Mind/Brain Sciences, University of Trento, Rovereto, Italy
[2]Department of Physics, University of Trento, Trento, Italy

* Corresponding author: albrecht.haase@unitn.it

Synaptic boutons are highly plastic structures undergoing experience-dependent changes in their number, volume, and shape. Their plasticity has been intensively studied in the insect mushroom bodies by counting manually the number of boutons within small regions of interest and extrapolating this number to the volume of the mushroom body neuropil.

Here we extend the analysis of synaptic bouton distributions within the mushroom body neuropil of honey bees (*Apis mellifera*) beyond sampling small volumes. This study, based on large 3D two-photon imaging combined with advanced image post-processing and multiple thresholds segmentation, suggests that previously reported results overestimated the number of synaptic boutons significantly. As a reason for that, we identified boundaries effects in the small volume samples. The application of the automated analysis to large volumes of the mushroom body neuropil revealed a corrected average density of synaptic boutons and, for the first time, their 3D spatial distribution. This distribution exhibited a considerable heterogeneity.

This additional information on synaptic bouton distribution provides new dimensions to future studies on brain development, symmetry, and plasticity.

Introduction

Since the French biologist Félix Dujardin first described the insect mushroom bodies (MBs)[1], these paired brain structures have been under intense investigations due to their involvement in multisensory processing, learning, and memory[2–5]. Structural and functional plasticity at their input region, the calyces, has been particularly studied in the past decade thanks to technological advances in fluorescence microscopy[6–9].

Within the MB calyces, synaptic boutons, called microglomeruli, are formed by the terminals of neurons coming from the first sensory brain centers and the dendrites of MB neurons[4,10,11]. The number of microglomeruli has been shown to vary in response to sensory stimulations[12–15], to memorization of olfactory information[13,16], and to aging[17,18]. Such variations have consequences on cognitive performance[19–21].

In all these studies, counting was performed manually in small regions of interest (ROIs) after immunostaining the synapsin, which is a protein located in the axon terminals of neurons[18]. Manual counting is an adequate method to study relative changes in the microglomerular density. However, besides being time-consuming, it is subjective and therefore requires a blinded analysis. It is also prone to errors since it assumes that microglomeruli are homogeneously spread within the MB calyx by using small ROIs to estimate an overall average density[22]. Due to the absence of an efficient automated analysis of larger ROIs, information about the spatial distribution of microglomeruli within the MB calyx has been missing.

A few automated methods have been suggested but were either applied to small ROIs[23] only, or their performance has been seriously questioned[24,25] because the absolute numbers of microglomeruli they provided strongly deviated from previously reported ones. An obvious limitation of automated counting is the vicinity of microglomeruli within the MBs, which is at the resolution limit of those microscope objectives that would allow imaging larger regions of the MBs. Moreover, the heterogeneity of fluorescent dye distribution after immunohistochemical staining of whole-mounted brains prevents simple standard segmentation algorithms to obtain accurate counting results.

The objective of this study was to quantify microglomeruli in larger regions of interest in the MB neuropil via an automated analysis. The automated procedure reduced subjectivity and greatly accelerated the evaluation. Beyond that, the technique provided completely novel information on the 3D distribution of microglomeruli in the olfactory neuropil of the MBs called the lip. This allows to search for stereotyped patterning in the microglomerular density and to study the heterogeneity of plastic changes induced by different learning paradigms.

Results and Discussion

Consistent number of microglomeruli obtained with the automated counting in ROIs

A major obstacle to the development of automated methods quantifying microglomeruli numbers has been the high vicinity of microglomeruli within the MB neuropil. Besides increasing the *z*-resolution by two-photon microscopy[26], the most important improvement in separability of microglomeruli in the present study was obtained by applying a 3D deconvolution to the raw data using the precisely measured point spread function of the microscope (Fig. 1). The resulting resolution of the lip images was sufficient to apply an automated analysis of microglomerular number using multiple thresholds segmentation.

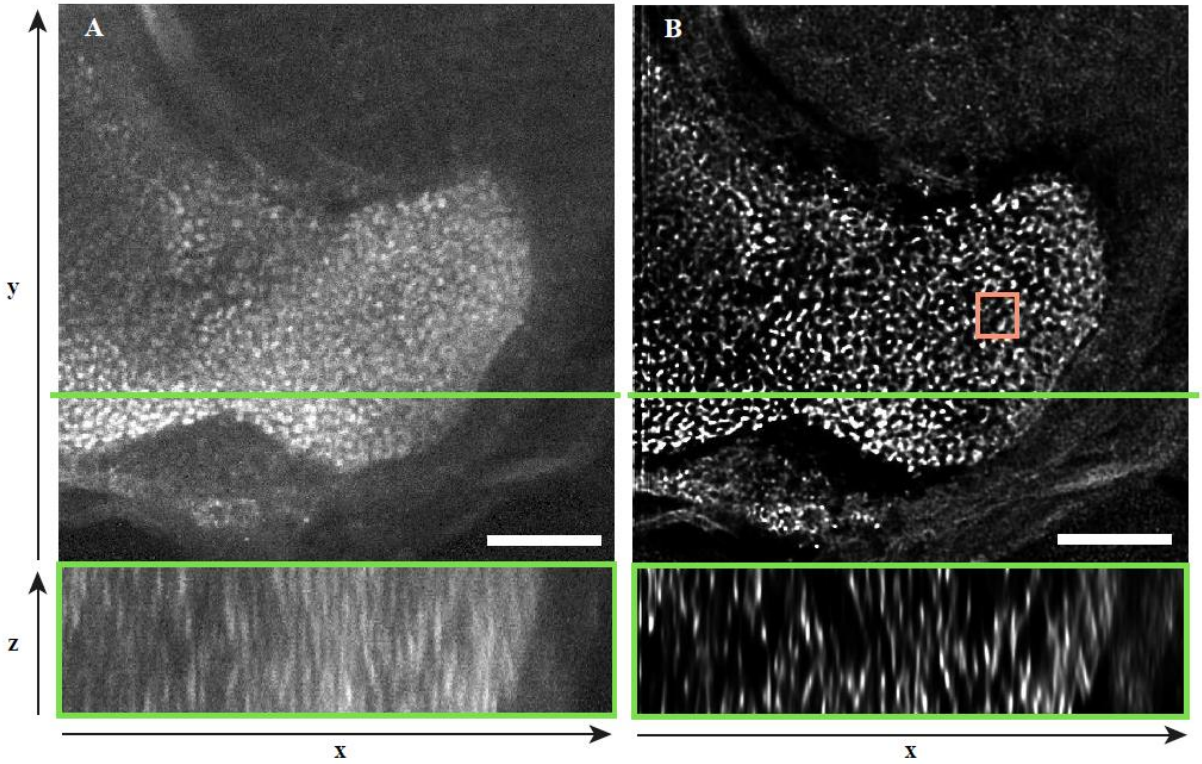

Figure 1. Post-acquisition processing of synapsin-immunolabeled brain images. Single two-photon microscopy sections of the right median MB lip are displayed before **(A)** and after **(B)** deconvolution and resampling. The upper panels represent frontal sections with the green line highlighting the position used to display the transversal sections in the lower panels. The square in (B) represents the ROI (10×10×10 µm) used to compare the manual and automated quantification methods. Scale bars are 100 µm.

The automated method gave a number of microglomeruli comparable to the one obtained by manual counting in 1000 µm^3 cubic ROIs within the MB lip (Fig. 2). A statistical analysis did not show a significant difference between the two methods (paired *t*-test; $t = -1.34$, $p = 0.22$, $n = 10$). This is the first validation of an automated method for the quantification of microglomerular numbers by direct comparison with the established manual method.

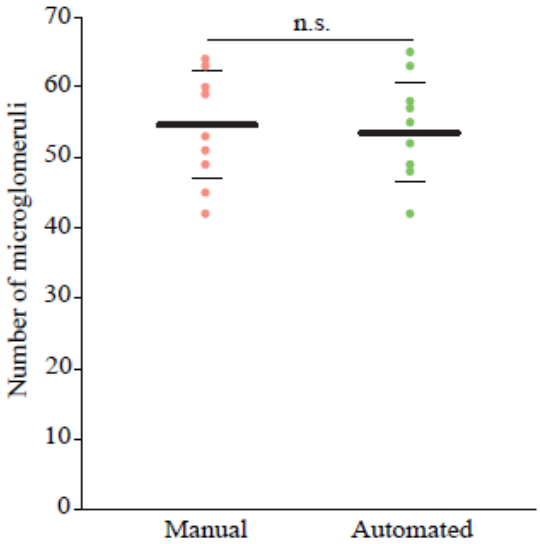

Figure 2. Comparison of the number of microglomeruli quantified with the automated and manual methods in a ROI (10×10×10 µm) positioned within the MB lip of different bees. The number of microglomeruli counted with the manual method (orange) did not differ significantly from the number obtained with the automated method (green) (paired *t*-test; $t = -1.34$, $p = 0.22$). The thick bars represent the mean number of microglomeruli counted with each method and the thin bars the standard deviations ($n = 10$).

The results obtained with the automated method were also consistent with the values obtained in the literature by manual counting in bees of similar age (Table 1). This was not the case of previously suggested automated methods[24,27]. Peng and Yang[24] obtained values 18-fold lower than the ones obtained by manual counting in 1000 µm^3 ROIs (Table 1). This may have been due to improper segmentation methods and the insufficient depth resolution of 5 µm between slices[25]. Indeed since the diameter of microglomeruli ranges on average[18] from 2.5 µm^3 to 4 µm^3, their coarse depth sampling may have overlooked several boutons. Also, the resolution limit of confocal microscopes along the *z*-axis falls in that range, which might have caused failure to separate neighboring microglomeruli. A limit that was overcome by our advanced post-acquisition processing of the MB lip images (Fig. 1), which

greatly improved image resolution and was fundamental for automated discrimination of microglomeruli.

Reference	Bee age	Method	Mean number / 1000 µm^3	Mean number / Lip
Groh et al. (2012)[18]	35 days	Manual	32.9	15.8×10^4
Münz et al. (2015)[17]	7 days		46.7	23.8×10^4
Münz et al. (2015)[17]	32 days		35.6	19.1×10^4
Sommerlandt et al. (2016)[21]	Unknown		36.3	15.9×10^4
Cabirol et al. (2017)[14]	10 days		48	18.5×10^4
Cabirol et al. (2018)[19]	24 days		69.4	32×10^4
Krofzic et al. (2008)[27]	37 days	Automated	358.7	NA
Van Nest et al. (2017)[23]	35 days		40.3	NA
Peng & Yang (2016)[24]	Unknown		1.9	0.4×10^4
Wolschin et al. (2009)[28]	5 days of foraging		40	NA
Present study	10 days		53.5	12.7×10^4

Table 1. Microglomerular density in the lip of honey bees reported in the literature. Manual and automated counts of synapsin-positive boutons in ROIs of 1000µm^3 positioned within the lip are compared between studies. For the manual method, the number of microglomeruli counted in the ROIs of 1000 µm^3 was extrapolated to the volume of the whole lip. Studies performed on bees with an age similar to the present study are highlighted (grey). Adapted from Rössler *et al.* (2017)[25].

From ROIs to the whole lip region

Previous manual methods considered a linear relationship between the number of microglomeruli and the volume of the ROIs in which they were counted. It became a standard to extrapolate measurements from the 1000 µm^3 ROIs to the volume of the whole MB subregion[18]. The problem of this procedure is the inclusion of microglomeruli whose centers fall inside the ROI but not their entire volume. What seems a negligible inaccuracy, sums up to a significant error during the extrapolation. This error could be quantified by applying the automated method to increasing ROI volumes (Fig. 3A). The number of microglomeruli showed a drastic deviation from a linear scaling with volume. A boundary-corrected model, which assumes that the number of microglomeruli cut by the ROI boundaries scales with the surface area of the ROIs (see Materials and methods), fitted the data nicely. Furthermore, it shows that the automated counting applied to a lip subregion (40 µm depth) agrees precisely with the predicted number from the boundary-corrected model (Fig. 3A inset). It proves that the high accuracy of automated counting is conserved also for large volumes, where a comparison with manual counting is not possible.

This allowed for a corrected estimation of the number of microglomeruli in the whole lip, showing that a linear extrapolation of numbers obtained in 1000 µm^3 ROIs overestimated the correct number on

average by 100% (Fig. 3B) (significant by *Wilcoxon test*; $W = 55$, $p < 0.005$, $n = 10$). This overestimation must be assumed for all the previously reported values obtained with the standard manual counting method in 1000 µm^3 ROIs. Table 1 provides an overview of the corresponding studies. For bees with an age equivalent to the ones used by us (10 days), manual counting indeed reported a considerably higher number of microglomeruli in the whole lip although the values in 1000 µm^3 ROIs were slightly smaller (Table 1, highlighted lines). The number of microglomeruli in the lip has been shown to decrease in older bees due to the synaptic pruning associated with foraging onset[17,19]. Yet, the number of microglomeruli reported in the whole lip of old foraging bees was similar to the one obtained in the present study in 10-day-old bees, while it was lower in 1000 µm^3 ROIs.

To avoid an overestimation of the density when counting in small ROIs, boutons that are partially outside the ROI should be counted only as fractions of one, corresponding to the percentage of their volume that lies inside the ROI. This significantly complicates and decelerates the already slow procedure and is another strong argument for automated counting over larger volumes.

The boundary effect became negligible for larger volumes (>10^5 µm^3) (Fig. 3A). It is therefore not required to determine the boundary-corrected fitting function, but a linear extrapolation of the number of microglomeruli in these volumes to the whole lip produces neglectable deviations with respect to variation across animals (*t*-test; $t = 0.64$, $p = 0.53$, $n = 10$) (Supplementary Fig. S1). This result confirms that applying the automated method to a subregion of 40 µm depth is sufficient to estimate efficiently the absolute number of microglomeruli in the whole lip.

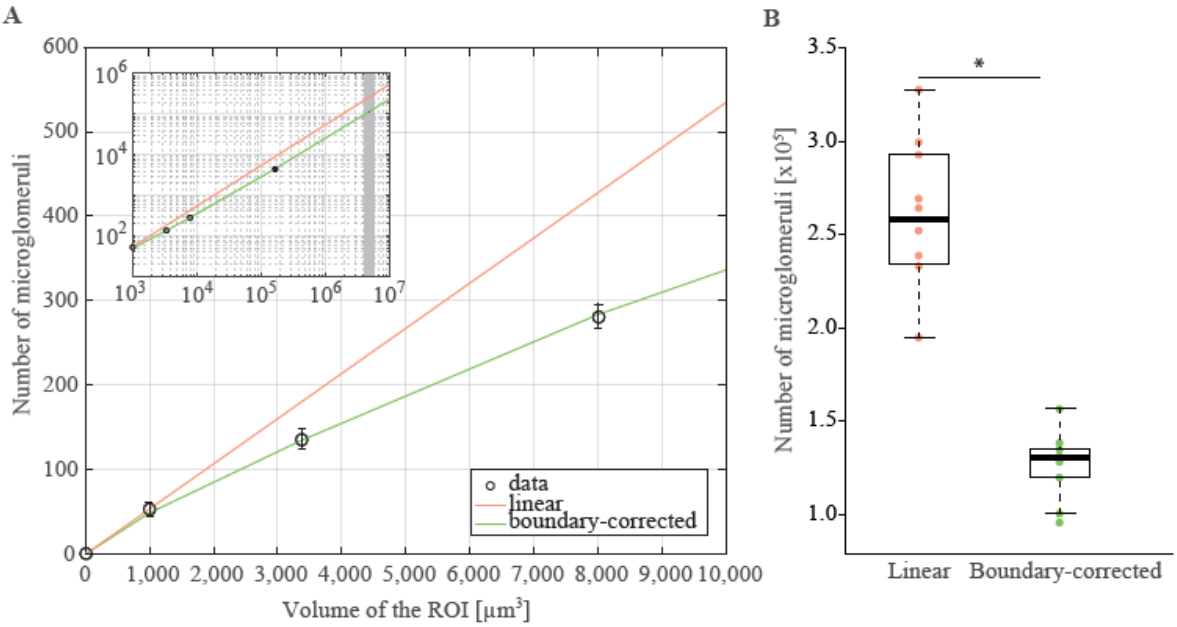

Figure 3. Comparison of the microglomerular number estimated in the whole MB lip with two models. (A) The variation in the number of microglomeruli counted inside a ROI with the volume of

this ROI was described by fitting two models (lines) to experimental data obtained via automated counting (open circles). The linear model (orange), used in previous studies, consisted of a linear extrapolation of microglomerular numbers counted in ROIs of 1000 μm^3 to the volume of the whole lip. In the boundary-corrected model (green), numbers measured as a function of ROI volume were fitted with a function that assumes the boundary effects to scale like the ROI surface area. For large volumes analyzed with automated counting (filled circle in the inset), boundary effects became negligible and the volume dependence became linear. The vertical bar in the inset (grey) represents the volume range of the whole lip. **(B)** The number of microglomeruli estimated by the two models in the whole lip differed significantly. The linear model overestimated the number of microglomeruli in the whole lip compared to the boundary-corrected model (Wilcoxon test; $W = 55$, $p = 0.002$, $n = 10$). Error bars represent the standard deviation, $*p = 0.002$.

Heterogeneous spreading of microglomeruli within the lip

Advanced image processing, based on 3D deconvolution, strongly improved the quality of our images acquired with a 20× objective (Fig. 1). This allowed avoiding the use of high magnification objectives, which are not suitable for an analysis of large volumes of the MB due to their small working distance and the small field of view. Thanks to the extended volume data, we were able to analyze for the first time the spatial distribution of microglomeruli in a subregion of the MB lip (Fig. 4A) and to measure their local density (Fig. 4B-D). The data revealed a substantial heterogeneity of the microglomerular distribution within the lip in all 3 dimensions.

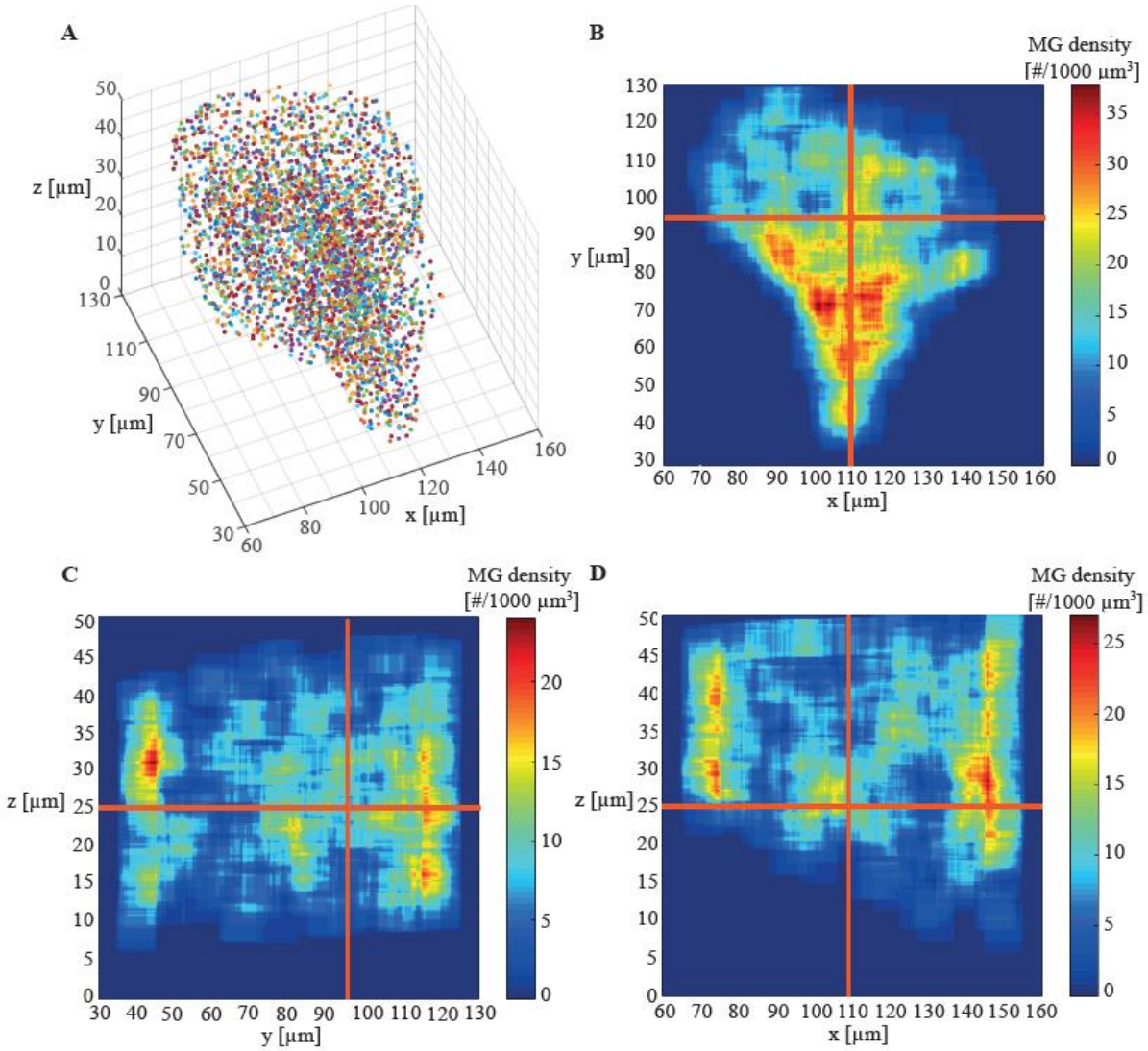

Figure 4. Spatial distribution of microglomeruli identified within the right median MB lip of one individual using the automated method. (A) The central coordinates of microglomeruli (colored circles) were used to visualize their 3D distribution in the lip (random colors for visual discrimination) **(B-D)** The density of microglomeruli in #/1000 µm^3 was obtained by a running average, using a volume element of that size. This revealed the heterogeneity in the microglomerular distribution in all dimensions of the MB lip. The red lines represent the focal planes used to display all 3 dimensions.

This exposed a further shortcoming of counting microglomeruli in 1000 µm^3 ROIs, which is prone to large fluctuation depending on the ROI position. Therefore, the absolute numbers of microglomeruli in the MB neuropils reported in previous studies with manual counting need to be taken with care, and data should be revised.

When smaller structures need to be described (*e.g.* individual synapses), higher resolution and higher magnifications are required. Until now, this has mainly been achieved using electron microscopy[8,29–31]. However, new advances in light microscopy, in particular, the development of nanometer-resolution

microscopes, will allow for future optical studies down to the synaptic level[32]. Still, the described problem of boundary effects, being a general phenomenon, will be relevant also for those applications. Even in completely different scenarios, whenever objects of an extended size are counted within small sample volumes, a linear extrapolation of these counts should be examined critically for potential biases from boundary effects, as reported in this study.

Conclusions

Thanks to an automated quantification of synaptic boutons over large brain volumes, the present study avoided two biases that were identified in previous methods: **(i)** it does not require extrapolation from small volume regions where counting is sensitive to boundary effects and **(ii)** it reveals and considers the heterogeneous spreading of boutons in the brain structure.

The method is not only useful to correct previously obtained absolute densities, but it will open the door to studies on spatial patterning of synaptic boutons in the mushroom body, looking *e.g.* into the stereotypy of these patterns, their symmetry[33], and their plasticity.

Materials and methods

Animals

Experiments were performed in June 2018 on a honey bee colony (*Apis mellifera*) maintained at the University of Trento in Rovereto. Inter-individual variability in brain structure was reduced by using same-age honey bees reared under controlled conditions. For this, a comb of brood about to emerge was taken from the hive and left in complete darkness in an incubator (34°C, 55% humidity) overnight. Newborn adult bees were collected in the following morning. They were placed in cages (8×5×4.5 cm, 15 bees per cage) in complete darkness in an incubator (34°C, 55% humidity) for 7 days with unlimited access to sucrose solution (50% w/w) and water. The sucrose solution and water were changed every two days.

Immunostaining of synapsin in whole-mount brains

The protocol used for the immunostainings is fully described in elsewhere[18]. The brains of 7-day-old honey bees (n = 10) were dissected in Ringer solution (130 mM NaCl, 5 mM KCl, 4 mM MgCl2, 5 mM CaCl2, 15 mM Hepes, 25 mM glucose, 160 mM sucrose; pH 7.2) and fixed overnight in 4% formaldehyde at 4°C on a shaker. Brains were rinsed in PBS (1 M; 3×10 min) and permeabilized successively in 2% PBS-Triton X100 (PBS-Tx; 10 min) and 0.2% PBS-Tx (2×10 min). Brains were blocked in 2% Normal Goat Serum (in 0.2% PBS-Tx) for 1 h at room temperature. They were then incubated with the α-synapsin antibody SYNORF1 for 3 days at 4°C on a shaker, rinsed in PBS (5×10

min), and incubated with the Goat anti-Mouse secondary antibody Alexa-488 conjugate for 3 days at 4°C on a shaker. Finally, the brains were rinsed in PBS (5×10 min) and dehydrated in an ascending ethanol series (30, 50, 70, 90, 95, 100, 100, 100%; 10 min each). Clearing and mounting were performed in methyl salicylate.

Image acquisition

Whole-mounted brains were imaged using a two-photon microscope (Ultima IV, Bruker) with excitation at λ = 780 nm (Ti:Sa laser, Mai Tai Deep See HP, Newport), using a 20× objective (NA 1.0, water immersion, Olympus)[34]. For volume measurements of the MB lip, image stacks of the right median calyx were acquired with a resolution of 512×512 pixels with pixel size of 1.03×1.03 µm. The inter-slice interval was 5 µm. For microglomerular quantification, a subregion of the outer lip of the right median calyx was imaged with a pixel size of 0.34×0.34 µm, over a depth of 50 µm and with an inter-slice interval of 0.5 µm. The intensity of the laser was compensated with depth.

Volume reconstruction of the MB lip

The volume measurements of the lip were semi-automatically performed using AMIRA (V5.4, Thermo Scientific). Using the SegmentationEditor, lip borders were manually defined every 5-6 slices and interpolated by the software. After carefully checking the accuracy of the delimitation on each slice, the volume of the lip was calculated using the MaterialStatistics function. The metadata was exported in XML-format for further statistical analyses.

Image processing for microglomerular quantification

To improve contrast and resolution of the image stacks, essential for robust discrimination of microglomeruli, images of the lip subregion were post-processed by a 3D deconvolution in AMIRA. The required Point Spread Function (PSF) of the microscope objective was measured using fluorescent beats (TetraSpeck, 0.1 µm, Thermo Fisher). The maximum-likelihood deconvolution algorithms required 100 iterations for sufficient convergence. Images were then resampled to a final voxel size of 0.1×0.1×0.1 µm (Fig. 1).

Quantification of microglomeruli

The manual and automatic methods for microglomerular quantification were first applied to ROIs of size 10×10×10 µm, positioned within the lip (Fig. 1B).

Manual counting was performed using the AMIRA LandmarkEditor by placing landmarks on visually identified microglomeruli (Fig. 5C).

The automated counting protocol was based on the idea that repeated image segmentation using varying threshold levels assures that all separate objects are extracted from the image at least once. They were counted exactly once, by removing objects of identical position. In details, the AMIRA

SegmentationEditor was used to label voxels whose signal intensity was above a certain threshold. The threshold was varied in repeated applications from 20% to 90% of the maximum image intensity in steps of 10% (Fig. 5A, B). Connected labeled voxels formed objects whose center coordinates and volumes were extracted using the RegionStatistics module and exported in XML-format for further analyses.

Via code written in MATLAB (R2018, MathWorks) (Supplementary Methods S2), objects larger than 10 μm^3 were removed from all threshold datasets, containing obviously multiple microglomeruli. A minimum size limitation of 0.05 µm was applied to the lowest threshold dataset only (20% of signal maximum), since connected objects separate and have reduced sizes when increasing the threshold. The identification of microglomeruli was performed by calculating the pair-wise 3D distance between all object centers. Objects below a distance of 0.8 µm were considered to represent the same microglomerulus. This parameter, as well as all the others involved, were optimized regarding the robustness with which the algorithm reproduced manual counting results for all samples (compare Fig. 5C, D).

The same automated method was then applied to images of the lip subregion. To remove ringing artifacts due to the deconvolution, 5 µm had to be cropped at the *z*-boundaries, resulting in a lip subregion of 40 µm depth. The volume of this lip subregion was calculated as described for the whole lip.

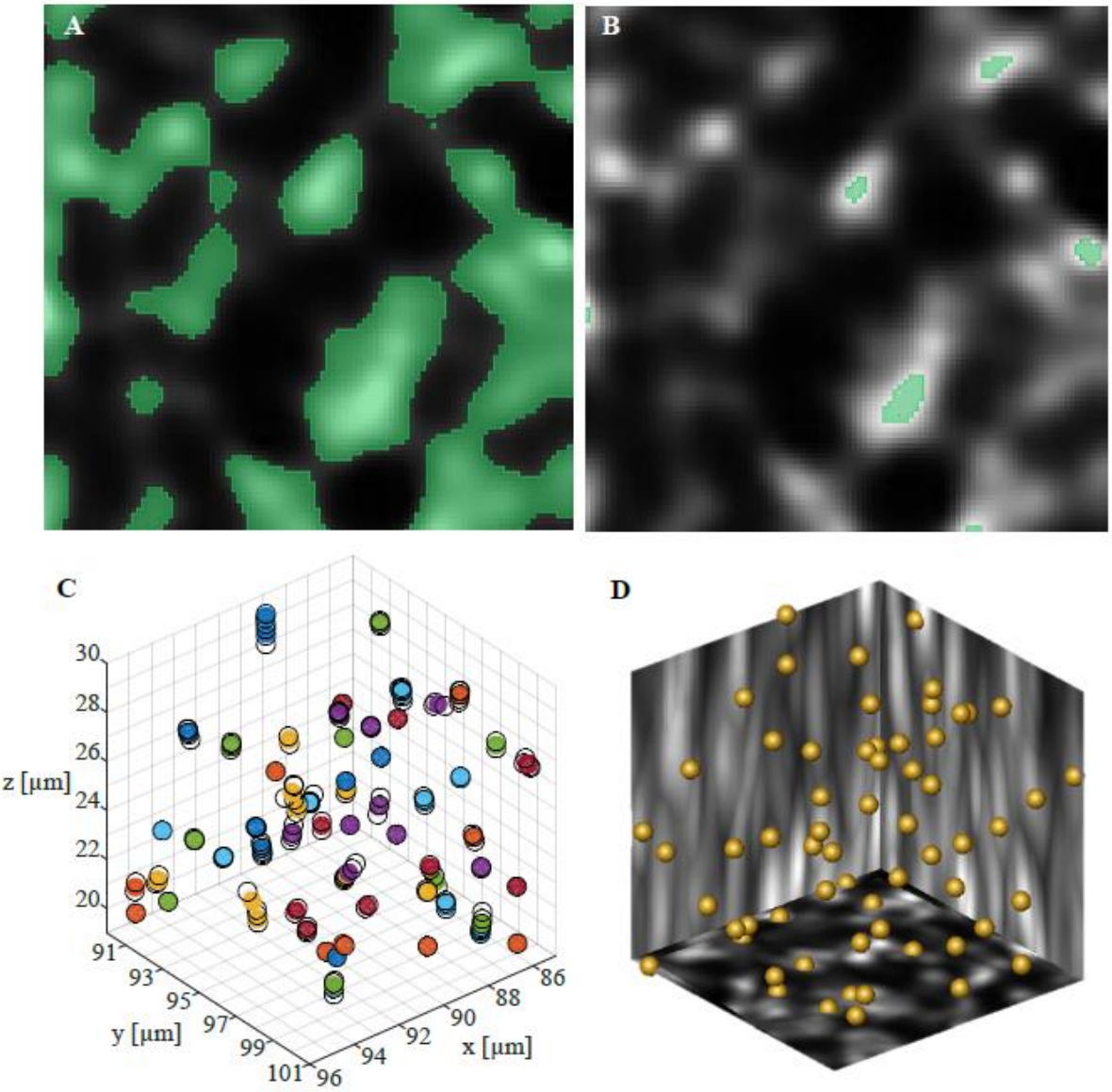

Figure 5. Quantification of microglomerular number in a ROI (10×10×10 µm) positioned within the MB lip. In the automated method, microglomeruli were identified as single connected regions with an intensity level above a defined threshold. An example shows a single section segmented with threshold 20% **(A)** and 90% **(B)** with respect to the maximum intensity (green labels mark intensities above threshold). **(C)** The central coordinates of these 3D connected regions (open circles) were compared and those with centers distant less than 0.8 µm were considered representations of the same microglomerulus (colored circles). **(D)** In the manual method, landmarks were placed on top of visually identified microglomeruli and automatically counted by the software.

Quantification of boundary effects when counting in ROIs

When counting microglomeruli in cubic ROIs, some microglomeruli are inevitably located at the boundaries of the ROIs. To evaluate the influence of boundary effects, ROIs of different volumes: 1000

μm^3 (10×10×10 μm), 3375 μm^3 (15×15×15 μm), and 8000 μm^3 (20×20×20 μm) were selected around the same center point. The included microglomeruli were counted with the automated method. Microglomerular numbers were averaged over different bees and their scaling as a function of ROI volume was analyzed by fitting two models.

A first model assumed that boundary effects were negligible and extrapolated the number of microglomeruli in the 1000-μm^3 ROI linearly with the volume:

$$N_1(V) = a\,V \tag{1}$$

A second model assumed that besides the number of microglomeruli entirely included in the ROI, which increases linearly with the ROI volume, there was an additional contribution of the microglomeruli partially cut by the ROI boundaries. These microglomeruli constitute a share proportional to the boundary area. Since the boundary surface area scales with the volume as $V^{2/3}$, the fitting function reads:

$$N_2(V) = a\,V + b\,V^{2/3} \tag{2}$$

This boundary effect will lose importance with increasing *V*, showing a linear scaling for high *V*. Comparing the real data to the two models allowed to evaluate whether the data actually deviated from the linear behavior and if so, to identify the ROI volume from which boundary effects became negligible.

Statistical analyses

The normality of data distribution was confirmed for all variables by applying a *Shapiro-Wilk test* ($p > 0.05$). The homogeneity of variances was assessed with a *Bartlett test*. Since both normality and homoscedasticity were verified, a paired *t*-test was used to compare the number of microglomeruli counted with the manual and automated methods in the ROIs of 1000 μm^3. Since variances between microglomerular numbers estimated in the whole lip by the two models were heterogeneous, a *Wilcoxon test* was used to compare these numbers.

References

1. Dujardin, F. Mémoire sur le système nerveux des insectes. *Ann. Sci. Nat. Zool.* **(3) 14,** 195–205 (1850).
2. Gerber, B., Tanimoto, H. & Heisenberg, M. An engram found ? Evaluating the evidence from fruit flies. *Curr. Opin. Neurobiol.* **14,** 737–744 (2004).
3. Menzel, R. & Manz, G. Neural plasticity of mushroom body-extrinsic neurons in the honeybee brain. *J. Exp. Biol*. **208,** 4317–4332 (2005).
4. Gronenberg, W. Subdivisions of hymenopteran mushroom body calyces by their afferent supply. *J. Comp. Neurol.* **435,** 474–489 (2001).
5. Menzel, R. The insect mushroom body, an experience-dependent recoding device. *J. Physiol.*

Paris **108,** 84–95 (2014).

6. Kremer, M. C. *et al.* Structural long-term changes at mushroom body input synapses. *Curr. Biol.* **20,** 1938–1944 (2010).

7. Szyszka, P., Galkin, A. & Menzel, R. Associative and non-associative plasticity in kenyon cells of the honeybee mushroom body. *Front. Syst. Neurosci.* **2,** 3 (2008).

8. Groh, C., Lu, Z., Meinertzhagen, I. a. & Rössler, W. Age-related plasticity in the synaptic ultrastructure of neurons in the mushroom body calyx of the adult honeybee Apis mellifera. *J. Comp. Neurol.* **520,** 3509–3527 (2012).

9. Faber, T. & Menzel, R. Visualizing mushroom body response to a conditioned odor in honeybees. *Naturwissenschaften* **88,** 472–476 (2001).

10. Groh, C. & Rössler, W. Comparison of microglomerular structures in the mushroom body calyx of neopteran insects. *Arthropod Struct. Dev.* **40,** 358–367 (2011).

11. Strausfeld, N. J., Hansen, L., Li, Y., Gomez, R. S. & Ito, K. Evolution, Discovery, and Interpretations of Arthropod Mushroom Bodies. *Learn. Mem.* **5,** 11–37 (1998).

12. Stieb, S. M., Muenz, T. S., Wehner, R. & Rössler, W. Visual experience and age affect synaptic organization in the mushroom bodies of the desert ant Cataglyphis fortis. *Dev. Neurobiol.* **70,** 408–423 (2010).

13. Falibene, A., Roces, F. & Rössler, W. Long-term avoidance memory formation is associated with a transient increase in mushroom body synaptic complexes in leaf-cutting ants. *Front. Behav. Neurosci.* **9,** 84 (2015).

14. Cabirol, A., Brooks, R., Groh, C., Barron, A. B. & Devaud, J. Experience during early adulthood shapes the learning capacities and the number of synaptic boutons in the mushroom bodies of honey bees (Apis mellifera). *Learn. Mem.* 557–562 (2017).

15. Scholl, C. *et al.* Light exposure leads to reorganization of microglomeruli in the mushroom bodies and influences juvenile hormone levels in the honeybee. *Dev. Neurobiol.* **74,** 1141–1153 (2014).

16. Hourcade, B., Muenz, T. S., Sandoz, J.-C., Rössler, W. & Devaud, J.-M. Long-term memory leads to synaptic reorganization in the mushroom bodies: a memory trace in the insect brain? *J. Neurosci.* **30,** 6461–6465 (2010).

17. Muenz, T. S. *et al.* Neuronal plasticity in the mushroom body calyx during adult maturation in the honeybee and possible pheromonal influences. *Dev. Neurobiol.* **75,** 1368–1384 (2015).

18. Groh, C., Lu, Z., Meinertzhagen, I. a. & Rössler, W. Age-related plasticity in the synaptic ultrastructure of neurons in the mushroom body calyx of the adult honeybee Apis mellifera. *J. Comp. Neurol.* **520,** 3509–3527 (2012).

19. Cabirol, A., Cope, A. J., Barron, A. B. & Devaud, J. Relationship between brain plasticity , learning and foraging performance in honey bees. *PLoS One* **13,** e0196749 (2018).

20. Li, L. *et al.* A possible structural correlate of learning performance on a colour discrimination

task in the brain of the bumblebee. *Proceedings. Biol. Sci.* **284,** 20171323 (2017).

21. Sommerlandt, F. M. J., Spaethe, J., Rossler, W. & Dyer, A. G. Does Fine Color Discrimination Learning in Free-Flying Honeybees Change Mushroom- Body Calyx Neuroarchitecture ? *PLoS One* **11,** e0164386 (2016).
22. Fahrbach, S. E. & Van Nest, B. N. Synapsin-based approaches to brain plasticity in adult social insects. *Curr. Opin. Insect Sci.* **18,** 27–34 (2016).
23. Van Nest, B. N., Wagner, A. E., Marrs, G. S. & Fahrbach, S. E. Volume and density of microglomeruli in the honey bee mushroom bodies do not predict performance on a foraging task. *Dev. Neurobiol.* **77,** 1057–1071 (2017).
24. Peng, Y.-C. C. & Yang, E.-C. C. Sublethal dosage of imidacloprid reduces the microglomerular density of honey bee mushroom bodies. *Sci. Rep.* **6,** 19298 (2016).
25. Rössler, W., Spaethe, J. & Groh, C. Pitfalls of using confocal-microscopy based automated quantification of synaptic complexes in honeybee mushroom bodies (response to Peng and Yang 2016)'. *Sci. Rep.* **7,** 7–11 (2017).
26. Haase, A. *et al.* In-vivo two-photon imaging of the honey bee antennal lobe. *Biomed. Opt. Express* **2,** 131 (2011).
27. Krofczik, S., Khojasteh, U., de Ibarra, N. H. & Menzel, R. Adaptation of microglomerular complexes in the honeybee mushroom body lip to manipulations of behavioral maturation and sensory experience. *Dev. Neurobiol.* **68,** 1007–1017 (2008).
28. Wolschin, F., Münch, D. & Amdam, G. V. Structural and proteomic analyses reveal regional brain differences during honeybee aging. *J. Exp. Biol.* **212,** 4027–4032 (2009).
29. Trujillo-Cenóz, O. & Melamed, J. Electron microscope observations on the calyces of the insect brain. *J. Ultrastruct. Res.* **7,** 389–398 (1962).
30. Seid, M. & Wehner, R. Ultrastructure and synaptic differences of the boutons of the projection neurons between the lip and collar regions of the mushroom bodies in the ant, Cataglyphis albicans. *J. Comp. Neurol.* **507,** 1102–1108 (2008).
31. Ganeshina, O. & Menzel, R. GABA-immunoreactive neurons in the mushroom bodies of the honeybee: An electron microscopic study. *J. Comp. Neurol.* **437,** 335–349 (2001).
32. Vicidomini, G., Bianchini, P. & Diaspro, A. STED super-resolved microscopy. *Nat. Methods* **15,** 173–182 (2018).
33. Haase, A. *et al.* A multimodal approach for tracing lateralisation along the olfactory pathway in the honeybee through electrophysiological recordings, morpho-functional imaging, and behavioural studies. *Eur. Biophys. J.* **40,** 1247–1258 (2011).
34. Paoli, M., Andrione, M. & Haase, A. Imaging techniques in insects. in *Neuromethods* (eds. Rogers, L. J. & Vallortigara, G.) **122,** 471–519 (Springer New York, 2017).

Additional information

Supplementary information accompanies this paper.

Competing financial interests: The authors declare no competing interests.

Author contributions

AC and AH designed research; AC performed research and analyzed data; AC and AH wrote the paper.

Acknowledgments

This work was funded by the Autonomous Province of Bolzano (Project B26J16000310003). The authors thank the members of the Neurophysics group of the Center for Mind/Brain Sciences & Department of Physics for useful comments on previous versions of the manuscript.